Chapter 3

In situ Reaction During Pulsed Nd:YAG Laser Welding SiC_p/A356 with Ti as Filler Metal

Kelvii Wei Guo

Additional information is available at the end of the chapter

http://dx.doi.org/10.5772/46087

1. Introduction

As aluminum matrix composites are generally low-cost and exhibit higher specific strength, high wearability, and good design performance property and functionality. They are widely applied in aerospace-flight, aviation structure, and automobile and in the heat resistant-wearable parts of engine [1-4]. Hence, a great deal of contemporary research effort is focusing upon their development and applications, typically on the discontinuously reinforced aluminum matrix composites like matrix with particle, short fiber, whisker and so forth. Additionally, a great deal of attention has also been drawn into the investigation of their secondary processing technologies like machining, joining and plastic forging. Welding is an important process for joining these materials. There has extensive effort to be devoted to developing appropriate process for joining the similar or dissimilar composites in literatures [2-4]. These processes can be mainly categorized as: (i) fusion welding like arc welding, shielding gas welding, laser welding and electron beam welding, *etc*.; and (ii) solid-state welding like soldering, explosive welding, friction welding and diffusion welding, *etc*. However, there still exist many problems in joining of the discontinuously reinforced aluminum matrix composites using conventional arc-welding processes and those high energy density welding methods like: laser welding and electron beam (EB) welding. These problems include: (i) the formation of poor weldment and the unsatisfactory properties of welded joints – mainly due to the high viscosity and poor flowability of the liquid welding pool causing mixing difficulty of the composite base material with filler materials; (ii) the occurrence of micro-segregation or inhomogeneous distribution of the reinforcement phases of SiC_p, Al_2O_{3p}, AlN and *etc*., and whiskers like SiC_w – typically owing to the rejection by their solidification front in the welding poor as cooling down, which subsequently prompts for many micro and macro defects in the weld and very poor

properties of the welded joints; (iii) the formation of aluminum carbide – mainly as a result of harmful interfacial reaction between aluminum matrix and reinforcement phases; and (iv) *so on.* A typical example of the interfacial reaction likely to have pernicious effects on the mechanical and chemical behavior of the composite is $4Al + 3SiC \rightarrow Al_4C_3 + 3Si$. This is owing to: (a) the formation of brittle and weak aluminum carbide Al4C3 in the interfacial reaction sacrifices the reinforcement-materials in the composite; and (b) the unstable aluminum carbide in wet environments causes corrosion of the composite because of its rapid hydrolysis *etc*.

Aiming at developing or improving the conventional welding technique, this paper studies the technique of welding the stir-cast aluminum matrix composite SiC_p/A356 by Nd:YAG laser welding with pure titanium as filler. This study has been specifically concerned on the *in situ* reinforcement effect of Ti on the microstructures of laser welded joints, which have been analyzed by means of Scanning Electron Microscope (SEM), Transmission Electron Microscope (TEM) and Electron Diffusion X-ray analysis (EDX) *etc*. The study aims at providing some ground works for further studies in this field.

2. Experimental material and process

2.1. Experimental material

Stir-cast SiC_p/A356 aluminum matrix composite, reinforced with 20 % volume fraction SiC particle of 12 μm mean size, was used as the welding specimens. The tensile strength of such specimens was 240 MPa and their solid-liquid phase transformation temperature was in the range of 562.6～578.3 ˚C. Figure 1 showed their corresponding microstructure while Table 1 tabulated the chemical composition of the A356 matrix alloy. Pure titanium was used as the filler metal.

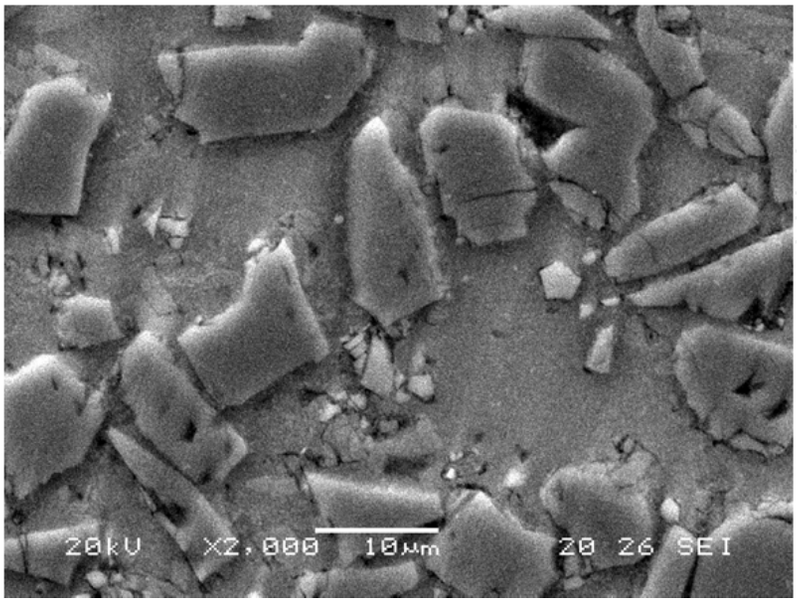

Figure 1. Microstructure of SiC_p/A356 aluminum matrix composite

Composition (Wt %)			
Si	Mg	Ti	Al
6.5~7.5	0.3~0.5	0.08~0.2	Bal.

Table 1. Composition of A356

2.2. Experimental process

The stir-cast aluminum matrix composite specimens were individually wire-cut to the size of 3 mm × 10 mm × 35 mm (Fig. 2). The quench-hardened layer induced by wire-cut and the oxide on the surfaces of specimens were polished away by 400 # emery cloth. The pure titanium filler was then machined to depth 3 mm × width 10 mm × thickness of 0.15 mm, 0.3 mm, 0.45 mm, 0.5 mm, 0.6 mm and 0.75 mm, respectively The specimens were then mounted into a clamping devise on the platform of a GSI Lumonics Model JK702H Nd:YAG TEM_{00} mode laser system, and their welding surfaces were properly cleaned by acetone and pure ethyl alcohol so as to remove any possible contaminant. The prepared pure titanium filler was also thoroughly cleaned and carefully sandwiched between the two composite specimens in the clamp. Thereafter, specimens were welded immediately by the Nd:YAG laser with wavelength of 1.06 μm, defocused distance of 10 mm so as to give a focus spot diameter of approximately 1.26 mm, laser fluence energy 2 J, frequency 25 Hz, and pulse duration 4 ms. In the welding, the relative moving speed of the laser and the welding pieces (i.e. feedrate) was set at 300 mm/min

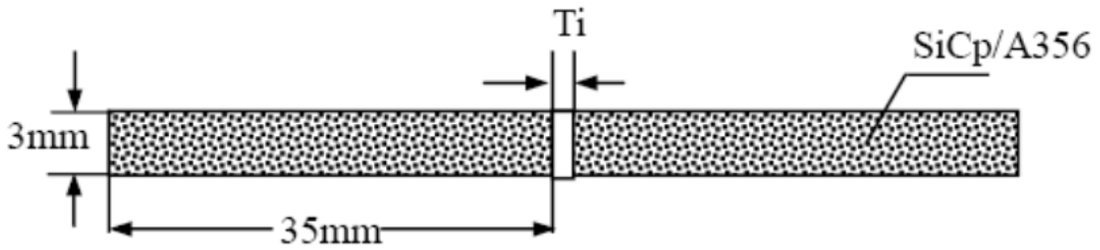

Figure 2. Schematic illustration of laser welding with Ti filler

Tensile strength of the joint was performed by a MTS Alliance RT/30 electron-mechanical material testing machine with a straining velocity of 0.5mm/min.The cross-section of welded joints was wire-cut for optical microscope investigation, and Scanning Electron Microscope (SEM) and Transmission Electron Microscope (TEM) analyses. SEM was used to analyze in detail the microstructure at the weld joints and the fractured tensile test-pieces of the joints. Optical microscope was used for observing the structure of a large area. TEM and Electron Diffusion X-ray analysis (EDX) were used to analyze the interface between the newly-formed phases and aluminum matrix, the distribution of chemical elements and spectra at the joints. The Nd:YAG laser with the similar setting conditions and feedrate was also used to weld the aluminum matrix composite specimens without any filler.

3. Results and discussion

3.1. Microstructures and properties of welded joints

The microstructure of the *in situ* reinforcement of Ti by Nd:YAG laser welding with 0.3 mm thick Ti filler was shown in Fig. 3. Appearance of *in situ* reinforcement particles distributed uniformly in the welded joint was seen. It also showed the disappearing of the drawbacks like incomplete fusion and pernicious phase Al4C3. These subsequently resulted in higher tensile strength (Table 2) of the joint. Comparatively, the reinforcement particles distributed more compactly than that of parent composite (cf. Fig. 1 and Fig. 3). The relatively more highly compacting reinforcement particles improved distinctly the properties of welded joints. The presence of Ti effectively improved the flowability of the liquid welding pool and the newly formed *in situ* reinforcement particles (Fig. 3) replaced those initial reinforcement particles (Fig. 1). Those dimples appeared in the SEM of the corresponding fractured surface (Fig. 4) suggested that: (i) the new-formed reinforcement particles had been perfectly wet; and (ii) the harmful composite structure of the initial welding viz. reinforcement/Ti/reinforcement had been changed to the state of reinforcement/matrix /reinforcement. XRD pattern of the fractured surface (Fig. 5) of the weld joint did not give sign of any harmful phase or brittle phase of Al4C3. This suggested the occurrence of effective interface transfers between reinforcement particles and matrix in the laser welded joint that subsequently provided favorable welding strength (Table 2). By the newly formed *in situ* reinforcement particles as detected by EDX (Table 3) and the intensity spectra shown in Fig. 5, the newly-formed reinforcement particle in the weld was identified as TiC.

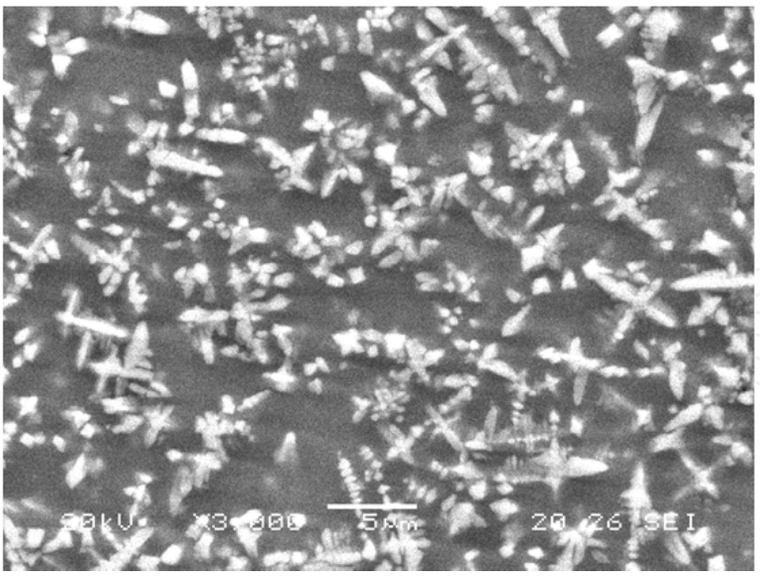

Figure 3. Microstructure of *in situ* reinforcement by laser welding with 0.3 mm thick Ti filler

Thickness of Ti filler (mm)	0.00	0.15	0.3	0.45	0.60	0.75
Mean strength (MPa)	76-91	126-135	168-180	143-160	107-113	79-96

Table 2. Mean tensile strength of laser welded specimens with various Ti filler thicknesses

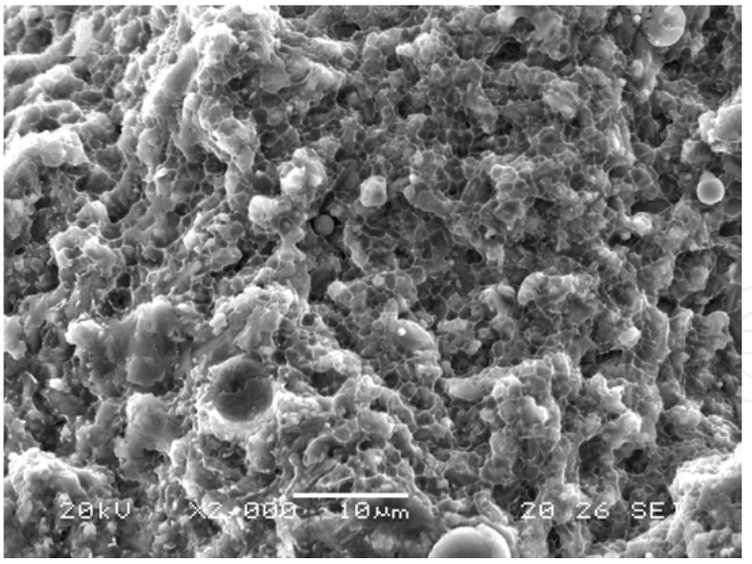

Figure 4. Fractograph of the laser welded joint with 0.3 mm thick Ti filler

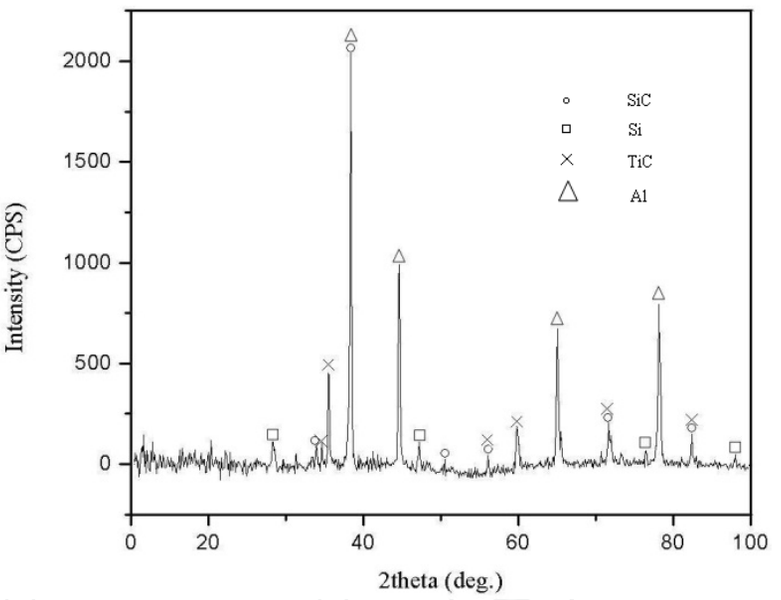

Figure 5. XRD pattern of the fracture surface for laser welding with 0.3 mm thick Ti filler

Element	Ti	Si	Al
Wt (%)	81.84	4.42	Bal.

Table 3. EDX analysis of newly-formed particle in the laser weld with 0.3 mm thick Ti filler

Figure 6. Macro-structure of the laser welded joint with 0.3 mm thick Ti filler

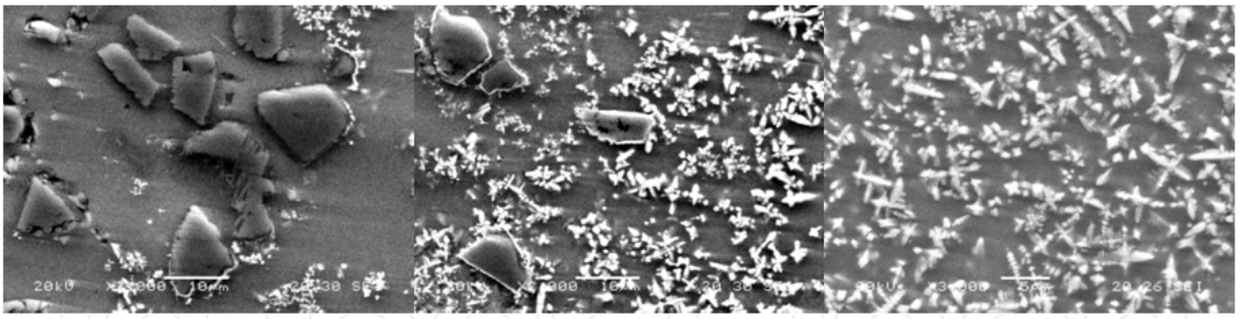

(a) (b) (c)

Figure 7. Microstructures of the different areas in the laser weld with 0.3 mm thick Ti filler (a) Area A (b) Area B (c) Area C

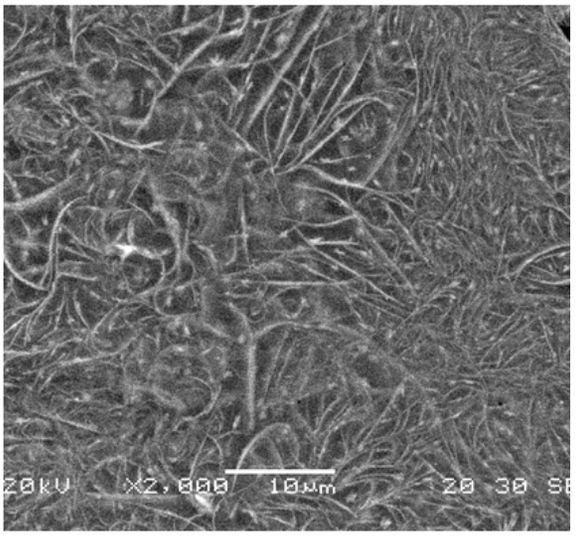

Figure 8. Microstructure of the weld with no-filler

Figure 6 illustrates the macro-structure of welded joint with Ti filler. Basically, the weld consisted of three main areas, namely: the *in situ* reinforcement area A, the two transitional areas B and C, and the no-*in situ* reinforcement area D. Their individual microstructures were shown in Fig. 7. The microstructures indicated the initial reinforcement SiC particles were completely replaced by the newly-formed *in situ* reinforcement TiC particles that mainly resulted in the formation of the *in situ* reaction area A (Fig. 7a). In the area B, the newly-formed *in situ* reinforcement TiC particles and the initial reinforcement SiC particles were coexistent (Fig. 7b). In the area C, very little newly-formed *in situ* reinforcement TiC particles were found (Fig. 7c). In the area D, there only existed the initial reinforcement particles SiC (Fig. 1). It was found that the typical pernicious acicular Al4C3 microstructure had been effectively alleviated in the welded area. Hence, it improved markedly the properties of the welded joints and their achievable tensile strength was up to 180 MPa (Table 2) that was about 75 % of the strength of SiCp/A356. The microstructure (Fig. 8) of the traditional Nd:YAG laser welding with no-filler showed that there were lots of pernicious acicular Al4C3 in the weld, which led to lower weld joint tensile strength (Table 2), i.e. only as high as 91 MPa (that was about 37.9 % of its parent SiCp/A356).

3.2. Element distribution in the transition area

Figure 9 illustrates the element distribution of the area B in the weld as shown in Fig. 6 and Fig. 7b. It showed the newly-formed *in situ* reinforcement particles were around the initial reinforcement SiC particles which offered a high density nucleus area for the nucleation of *in situ* TiC. The stirring effect in the welding pool by laser irradiation and the initial reinforcement SiC particles would be replaced by the newly-formed *in situ* TiC (cf. Figs 9b and 9c) following the chemical reaction process of:

$$Ti\,(l) + SiC\,(s) \longrightarrow TiC\,(s) + Si\,(s)$$

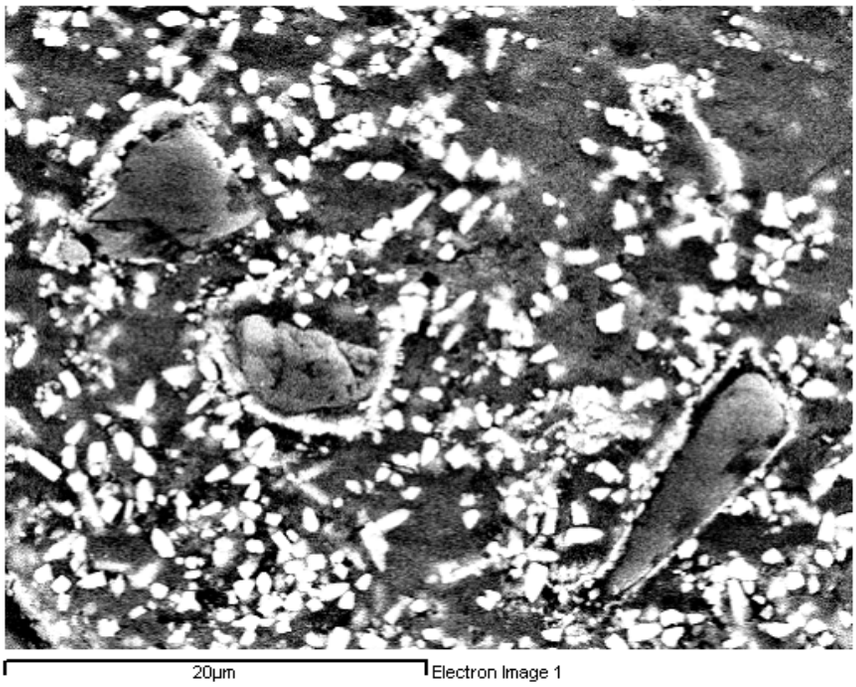

(a)

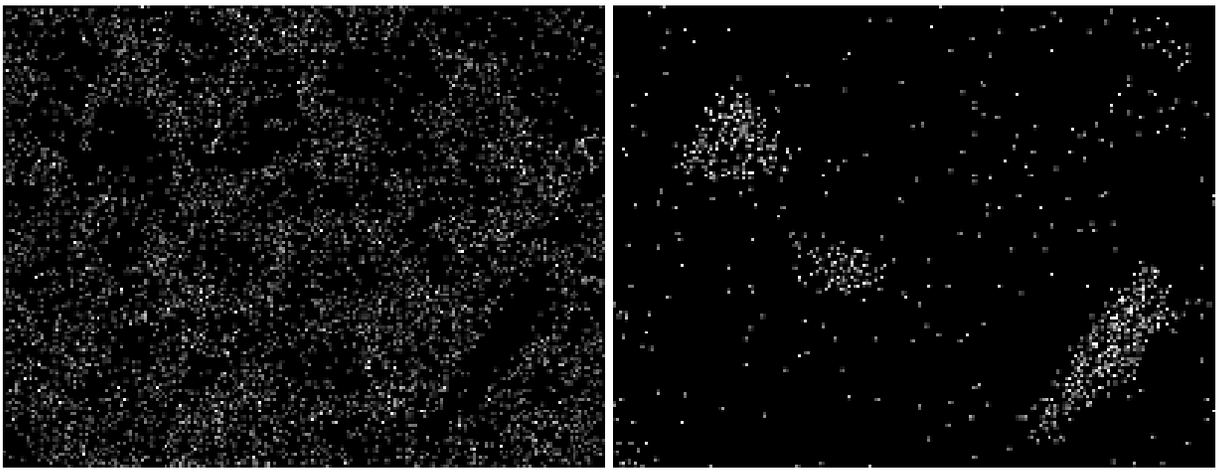

(b) (c)

Figure 9. Element distribution of B area in the weld; (a) micrograph of the area B (b) Ti element face distribution (c) Si element surface distribution

According to the free energy for forming the SiC, TiC and Al_4C_3 carbides as elaborated in Fig. 10 of literatures [5, 6, 7], the free energy required to form TiC was much lower than that for Al_4C_3 when the reaction temperature was above 800 ºC. The affinity between Ti and C in the Nd:YAG laser welding was therefore greater than that of Al and C. The chemical reaction between Ti and SiC in the welding pool would subsequently take precedence over the reaction between Al and SiC and thus resulted in restraining the formation of the pernicious acicular Al_4C_3.

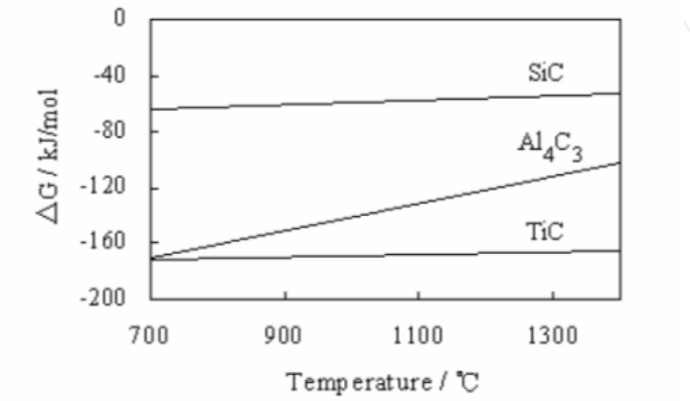

Figure 10. Free energy of formation of several metallic carbides [5, 6, 7]

3.3. Influence of Ti filler thickness

The microstructures of *in situ* reinforcement with various thicknesses of Ti filler were illustrated in Fig. 11 and its corresponding fractographs were shown in Fig. 12. It illustrated that the amount of the formed *in situ* TiC was distinctly increased with the increase in the thickness of Ti filler. Test indicated that maximum strength of welded joints (Table 2) was achieved at Ti filler thickness 0.3 mm (Figs. 3 and 4). This was because the newly-formed *in situ* reinforcement particles TiC were uniformly distributed in the weld and the initial irregular (mostly in hexagonal shape as shown in Fig. 1) reinforcement SiC particles in the weld were no longer observed (Fig. 3). Moreover, the pernicious acicular Al_4C_3 was successfully restrained (Figs 3 and 7a). At the thickness of Ti filler below 0.3 mm, there was little sign of the newly-formed *in situ* reinforcement TiC particles to be observed (Fig. 11a) and a number of pernicious acicular Al_4C_3 were formed in the weld. When the thickness of Ti filler was just beyond 0.3 mm, the properties of the joints tended to become poorer again (Fig. 12b). This was because the input energy was mainly used for melting the Ti filler and resulted in the coexistence of coarse columnar crystals and fine equiaxed crystals (Fig. 11b). When the thickness of Ti filler was further increased (Fig. 11c), the percentage of liquid Ti in the welding pool would also be increased. Subsequently, the weld zone would form coarser columnar crystals, as displayed in the SEM micrograph of Fig. 11c, after the resolidification of the melt. From the phase diagram (Fig. 13) of Ti-Al binary system [8], it can be anticipated that increasing the content of Ti would lead to the intermetallic compounds like TiAl and Ti_3Al, *etc*., to be

formed during the Nd:YAG laser welding. As illustrated by the XRD pattern of the fractured surface of a laser weld joint with the thicker Ti filler in Fig. 14, there were some distributing brittle intermetallic compounds like TiAl and Ti_3Al to be detected. Available literature [9] has demonstrated that TiAl and Ti_3Al are the harmful intermetallic compounds in the weld and tend to decrease obviously the strength of welded joints. Such harmful effect may follow the chemical reaction of: 5Ti[Al l] +3Al[l] + SiC[s]—→TiC[s] + Si[Al [l]] + Al[l] + (TiAl + Ti_3Al). Hence, too thick of the Ti filler led to: (i) the appearance of the large block of columnar crystals in the microstructure (Fig. 15); and (ii) the new-formed reinforcement TiC to be replaced by the melted/re-solidified Ti and subsequently only the melted/re-solidified Ti existing in the weld. Results (Figs 3, 7 and 11) indicated that there existed an optimal thickness of Ti filler in the individually set parameters in the Nd:YAG laser welding of SiCp/A356. With the optimal thickness of Ti filler, the initial reinforcement particles SiC distributed in the aluminum matrix composite SiCp/A356 would offer a highly dense nucleus area for the *in situ* TiC nucleation. This would effectively alleviate the forming of intermetallic compounds like TiAl and Ti_3Al in the weld. It was in this manner that ultimately created favorable condition to provide relatively superior strength of the welded joint to that of conventional laser welding.

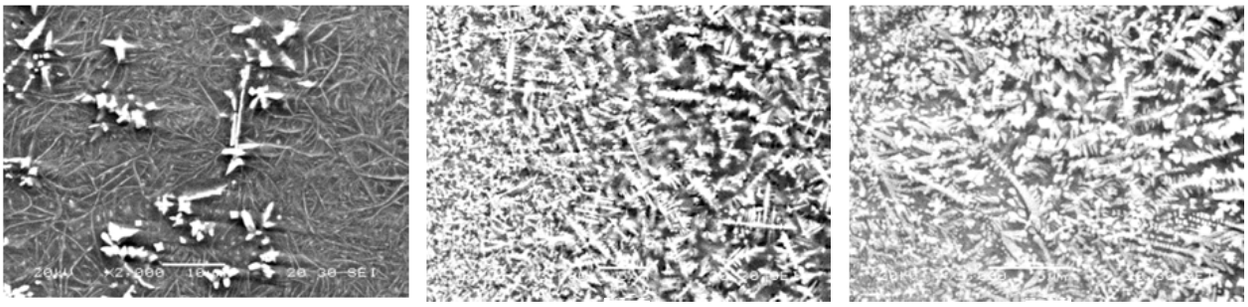

(a) (b) (c)

Figure 11. Microstructures in the A area with various thicknesses of Ti filler; (a) δ=0.15 mm (b) δ=0.45 mm (c) δ=0.60 mm

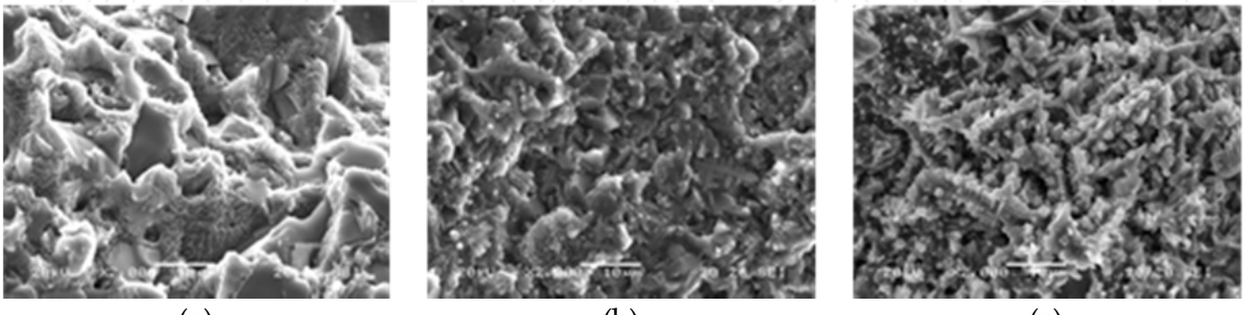

(a) (b) (c)

Figure 12. Fractographs of welded joints with various thicknesses of Ti filler; (a) δ=0.15 mm (b) δ=0.45 mm (c) δ=0.60 mm

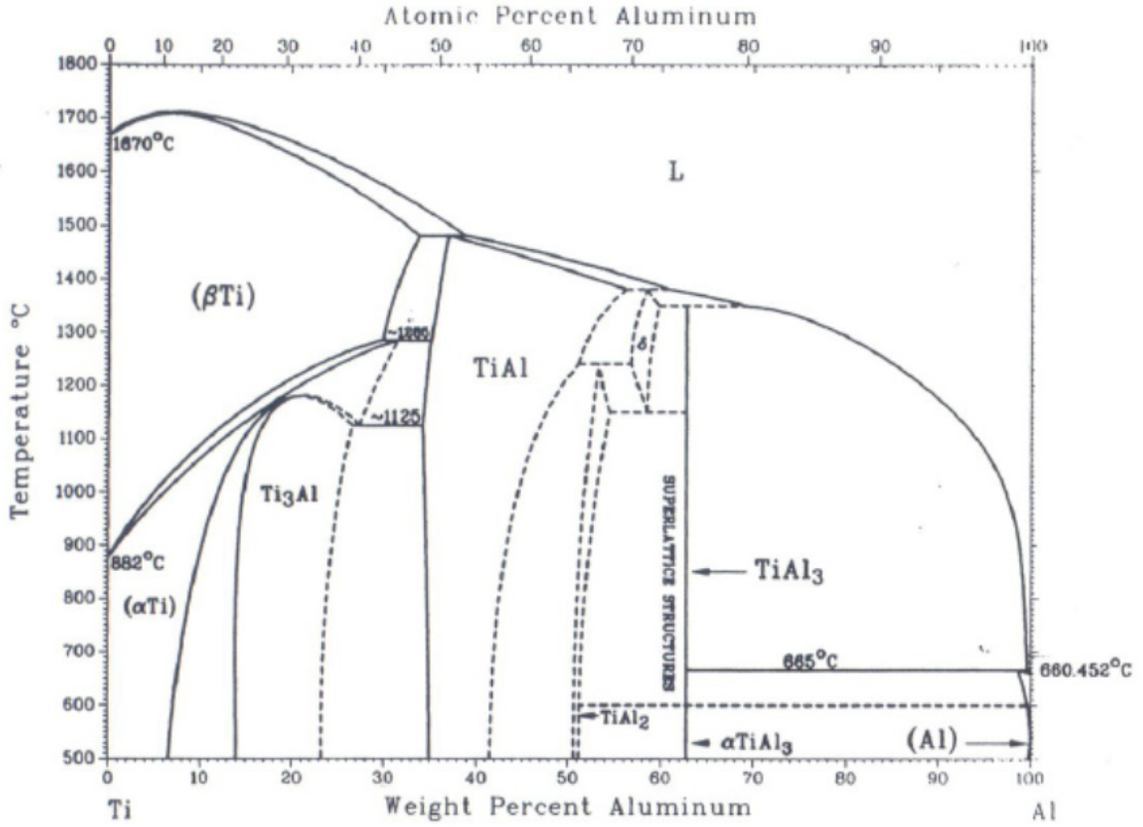

Figure 13. Binary phase diagram of Ti—Al [8]

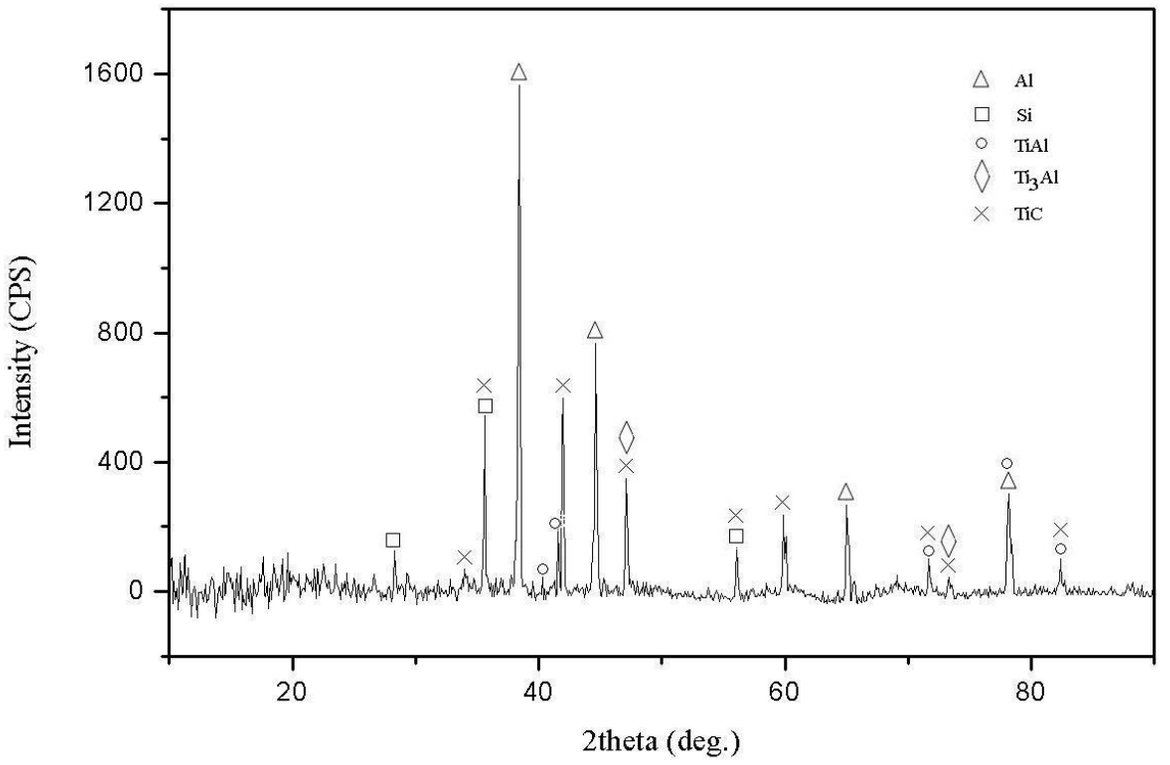

Figure 14. XRD pattern of fracture surface (δ=0.6 mm)

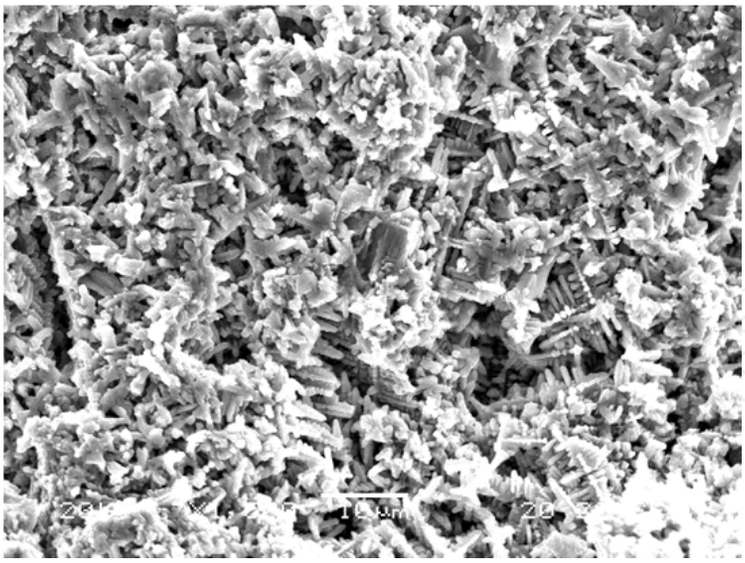

Figure 15. Columnar crystals in the laser weld with 0.6 mm thick Ti filler

3.4. TEM of the interface between *in situ* reinforcement particle TiC and matrix

The interface between *in situ* reinforcement particle TiC and the matrix was analyzed by the TEM micrograph displayed in Fig. 16. It demonstrated a clear interface between the newly-formed *in situ* reinforcement particle TiC and matrix. This clearly distinct interface (Fig. 16) suggested the occurrence of prominent *in situ* reaction to integrate the reinforcement particle with matrix (cf. Figs 4 and 16), and the high probability of successfully transferring load from the matrix to TiC and vice versa. It also gives indication that the aluminum matrix composite SiCp/A356 would be welded satisfactorily by Nd:YAG laser.

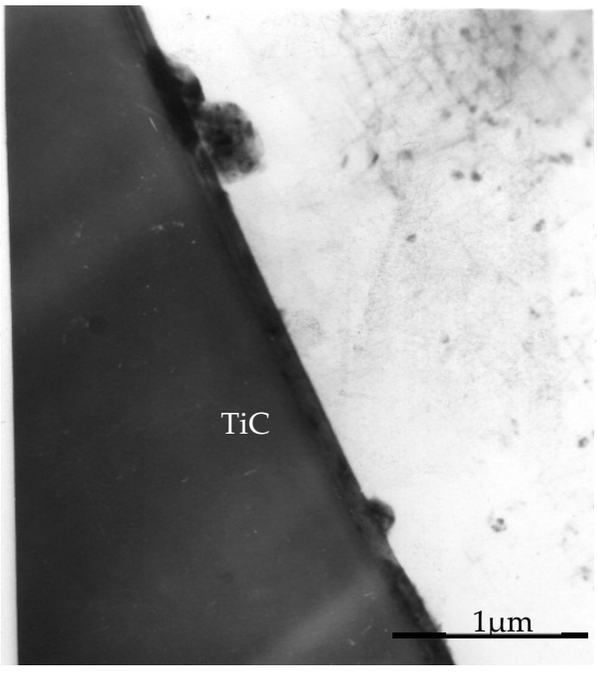

Figure 16. TEM of interface between *in situ* TiC reinforcement and the matrix for laser welding with 0.3 mm Ti filler

4. Microstructure evolution during the welding

4.1. Temperature field of laser welding

The heat is assumed to be released instantaneously at time t=0 on the surface of the substrate. This causes a temperature rise in the material as follows [10-12]:

$$T - T_0 = \frac{Q}{\rho c \left(4\pi\alpha t\right)^{\frac{3}{2}}} \exp\left(\frac{-R^2}{4\alpha t}\right) \tag{1}$$

where ρ is the material density, C is specific heat, α is thermal diffusivity, λ is thermal conductivity, Q is the input energy.

When temperature distribution is quasi-steady state:

$$T - T_o = \frac{q_o}{2\pi\rho c\alpha R} \exp\left(-\frac{v}{2\alpha}\left(R + x\right)\right) \tag{2}$$

During the Nd:YAG laser welding, q_0 can be expressed as

$$q_0 = \eta\left(N\left(f,v\right)\right) \times \frac{P}{\frac{\pi D^2}{4} \times PD} = \eta\left(N\left(f,v\right)\right) \times \frac{4P}{\pi D^2 \times PD} \tag{3}$$

Where

$\eta\left(N\left(f,v\right)\right)$ is the coefficient of laser welding input energy, which is direct proportional to number of overlaps or pulse frequency. With number of overlaps increasing, or pulse frequency increasing with constant the feed-rate, $\eta\left(N\left(f,v\right)\right)$ will be increased synchronously. With the velocity (feedrate) increasing, number of overlaps with the constant pulse frequency will be decreased correspondingly led to lower heat input, $\eta\left(N\left(f,v\right)\right)$ will be decreased accordingly.

Eq. (2) can be rewritten as:

$$T - T_o = \frac{2 \times \eta\left(N\left(f,v\right)\right) \times P}{\pi^2 D^2 \rho c\alpha R \times PD} \exp\left(-\frac{v}{2\alpha}\left(R + x\right)\right) \tag{4}$$

Define $\xi = \frac{1}{2\pi\rho c\alpha}$, then Eq. (4) can be written as:

$$T - T_o = \frac{\xi \times \eta\left(N\left(f,v\right)\right) \times P}{\frac{\pi D^2}{4} \times PD \times R} \exp\left(-\frac{v}{2\alpha}\left(R + x\right)\right) \tag{5}$$

$$\text{Define} \quad q = \frac{P}{\frac{\pi D^2}{4} \times PD}, \tag{6}$$

then Eq. (6) can be written as

$$T - T_o = \frac{\xi \times \eta\left(N\left(f, v\right)\right) \times q}{R} \exp\left(-\frac{v}{2\alpha}\left(R + x\right)\right) \tag{7}$$

4.2. Simulation model

4.2.1. Equations for temperature distribution

Using energy balance, a differential equation can be obtained for the steady temperature distribution in a homogeneous isotopic medium, that is

$$\frac{\partial}{\partial x}\left(K_x \frac{\partial \theta}{\partial x}\right) + \frac{\partial}{\partial y}\left(K_y \frac{\partial \theta}{\partial y}\right) + \frac{\partial}{\partial z}\left(K_z \frac{\partial \theta}{\partial z}\right) = -q^B \tag{8}$$

Where the boundary conditions are $\theta\big|_{s_1} = \theta_e$, $K_s \frac{\partial \theta}{\partial x}\Big|_{s_2} = q^s$.

For

$$\pi = \int_V \left\{ K_x \left(\frac{\partial \theta}{\partial x}\right)^2 + K_y \left(\frac{\partial \theta}{\partial y}\right)^2 + K_z \left(\frac{\partial \theta}{\partial z}\right)^2 \right\} d_V - \int_V \theta q^s d_V - \int_{s_2} \theta^s q^s d_s \tag{9}$$

After Eq. 9 is discrete for the element, and according to $\delta\pi = \sum_{e=1}^{n} \delta \pi_e = 0$, it will be obtained

$$\overline{K}\overline{\theta} = \overline{\theta_S} + \overline{\theta_B} - \overline{C\theta} + \overline{K^c}(\theta_C - \overline{\theta^s}) + \overline{K^r}(\theta_r - \overline{\theta^s}) \tag{10}$$

where *S*: isothermal boundary, *B*: the heat-input, *c*: the conductive and *r*: the irradiative.

4.2.2. Hypothesis and mesh

Based on the situations during the laser welding and mainly focused on the temperature distribution, it is supposed that the laser resource is considered as a Gaussian distribution. Also, on the basis of specimen size wire-cut, the calculating size is set as 25 mm (x) × 20 mm (y) × 3 mm (z), the schematic of its finite element (FE) mesh is shown in Fig. 17. Moreover, Ti filler is considered as a section of the substrate with the different properties to ignore the effect of gap between the Ti filler and the substrate.

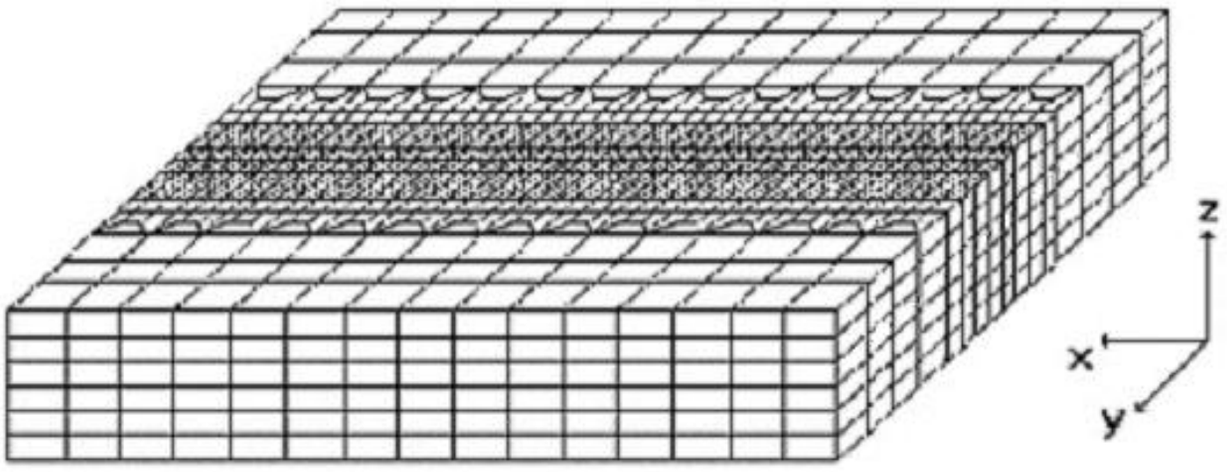

Figure 17. FE mesh for 3D numerical analysis

4.2.3. Temperature distribution

The simulated results are shown in Fig. 18 to Fig. 23. It shows that the temperature without Ti filler is same as the traditional laser welding. Simultaneously, due to the heat input into the substrates directly, without the additional heat resource for melting Ti filler, the peak of temperature (heat input) is relatively higher to form the weld. As a result, increasing the heat input into the substrate will decrease the tensile strength of the welded joint and wide the heat affected zone (HAZ) resulted in lower properties in the succedent practical applications (Table 2 and Fig. 19). Furthermore, a large amount of coarser acicular Al_4C_3 distributed in the fracture surface as shown in Fig. 19, which decreased the tensile strength of the welded joints seriously.

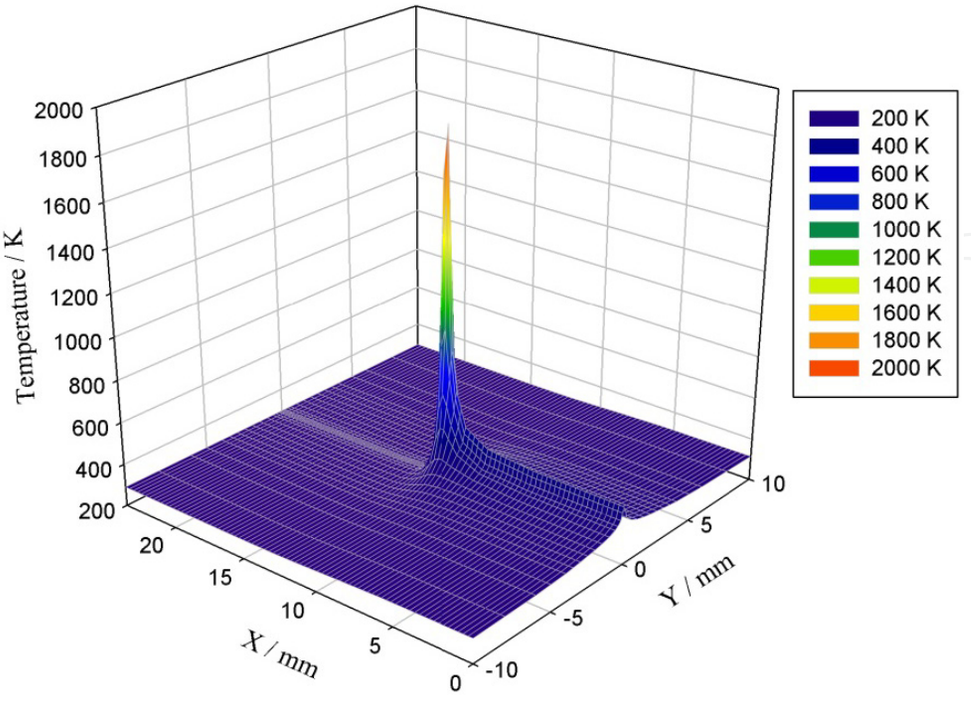

Figure 18. Temperature distribution without Ti filler

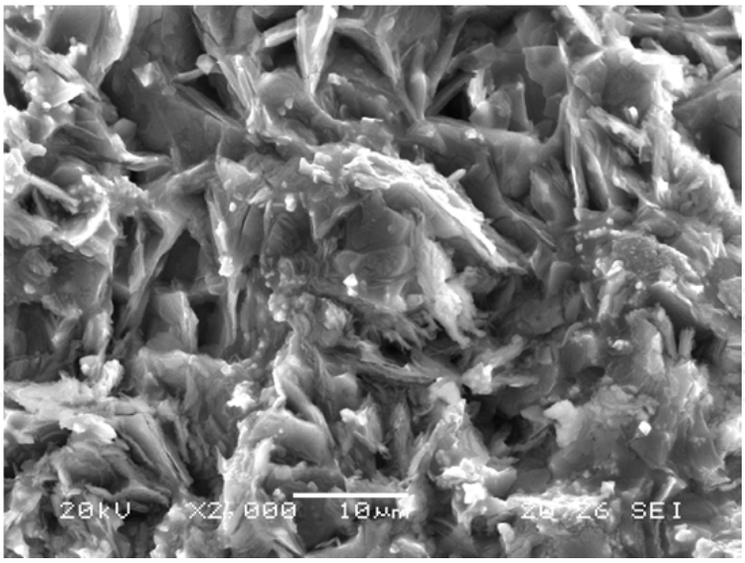

Figure 19. Fractograph of the laser welded joint without Ti filler

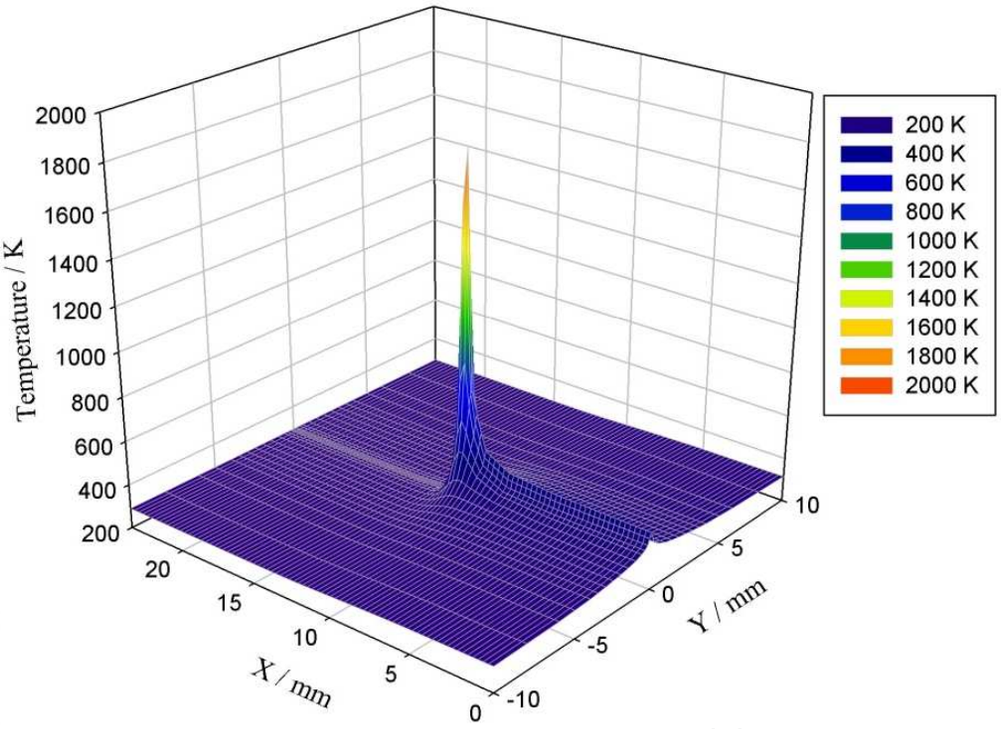

Figure 20. Temperature distribution with Ti filler

Figure 20 shows the temperature field of laser welding SiCp/A356 with Ti filler. Considering the Ti melting and *in situ* reaction in the welding pool as an endothermic reaction, the welding temperature decreases and will be lower than that of laser welding directly (cf. Figs. 18 and 20), and its temperature field is distributed more smoothly with *in situ* reaction than that of laser welding without Ti filler as shown in Fig. 21. Also, the width of HAZ is decreased to some extent (Fig. 21b). Furthermore, it shows that according to the real effect of laser beam diameter, the thickness of Ti filler is about 0.3 mm will be optimal for *in situ* welding which conformed to the experimental results as shown in Table 2.

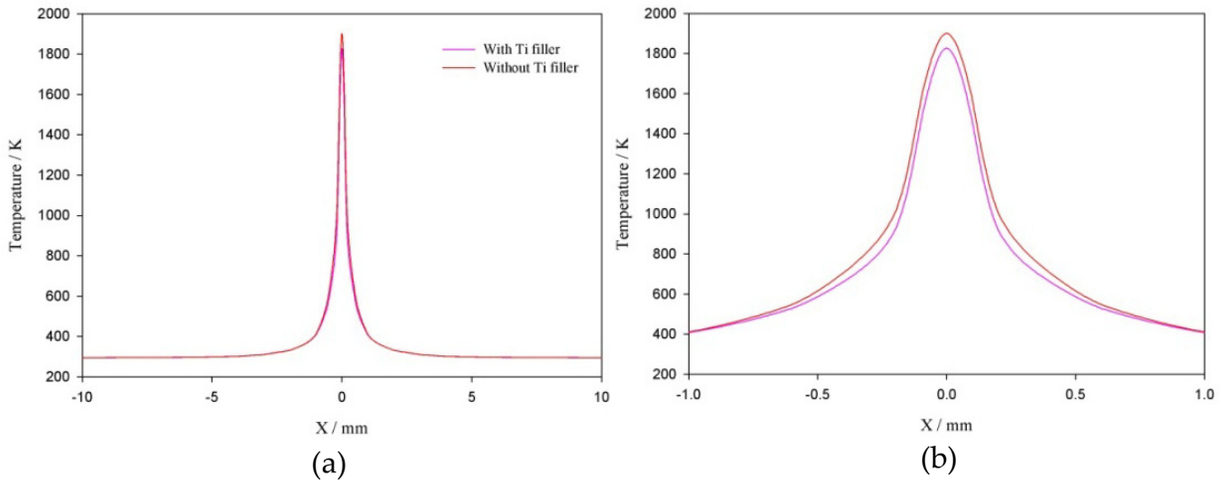

Figure 21. Temperature distribution of central heating on XOZ plane
(a) Temperature distribution on XOZ plane (b) Magnification of (a)

In addition, the effect of Ti on the temperature distribution on the central line is shown in Fig. 22. It illustrates that the peak of the temperature is changed distinctly. Because of the sandwiched Ti between the substrates and *in situ* endothermic reaction, the temperature of substrate ahead of laser resource is lower than that of without Ti filler. Moreover, the temperature at the succedent distance is increased or accumulated a little bit due to the different conductive coefficient between Ti and substrate. On the other side, its corresponding trend of the temperature behind the laser resource (resolidification) is same as that of without Ti filler except for a peak appearance induced by more serious exothermic potential during the crystallization.

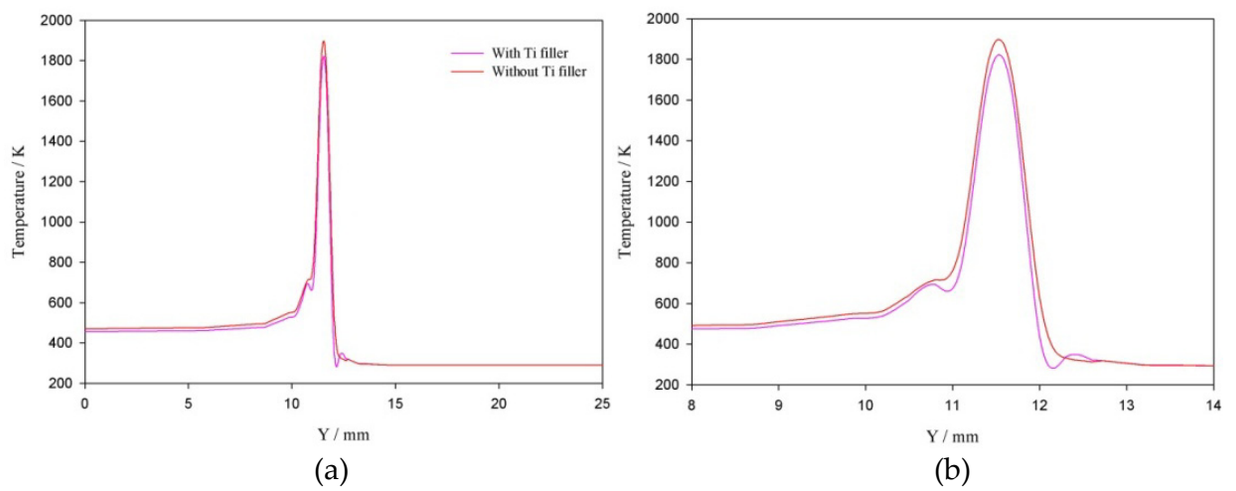

Figure 22. Temperature distribution of central line on YOZ plane
(a) Temperature distribution on YOZ plane (b) Magnification of (a)

Figure 23 shows the temperature distribution when Ti filler is thick. The peak of temperature is decreased obviously and leads to the welding failure.

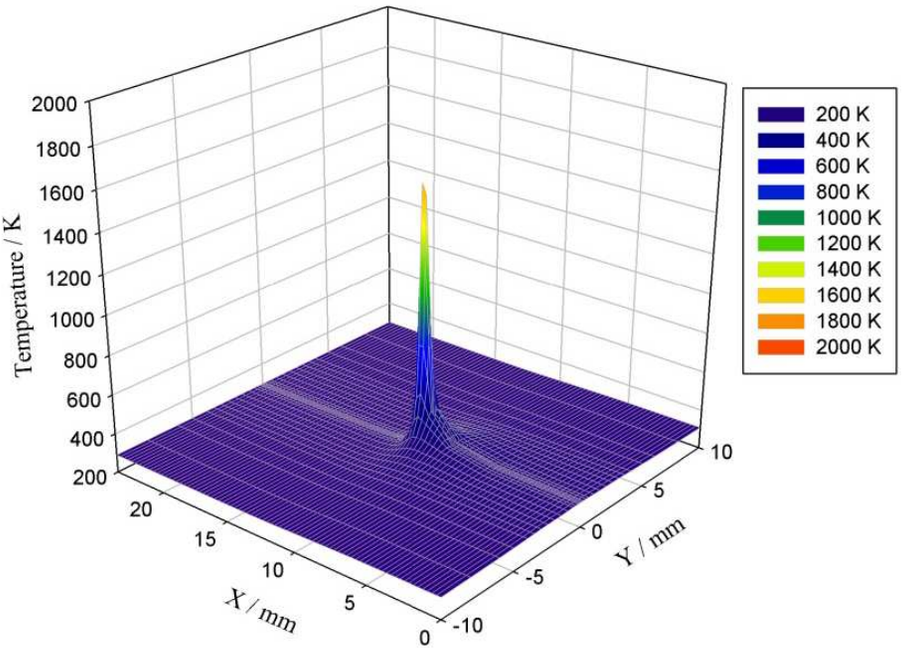

Figure 23. Temperature distribution with thick Ti filler

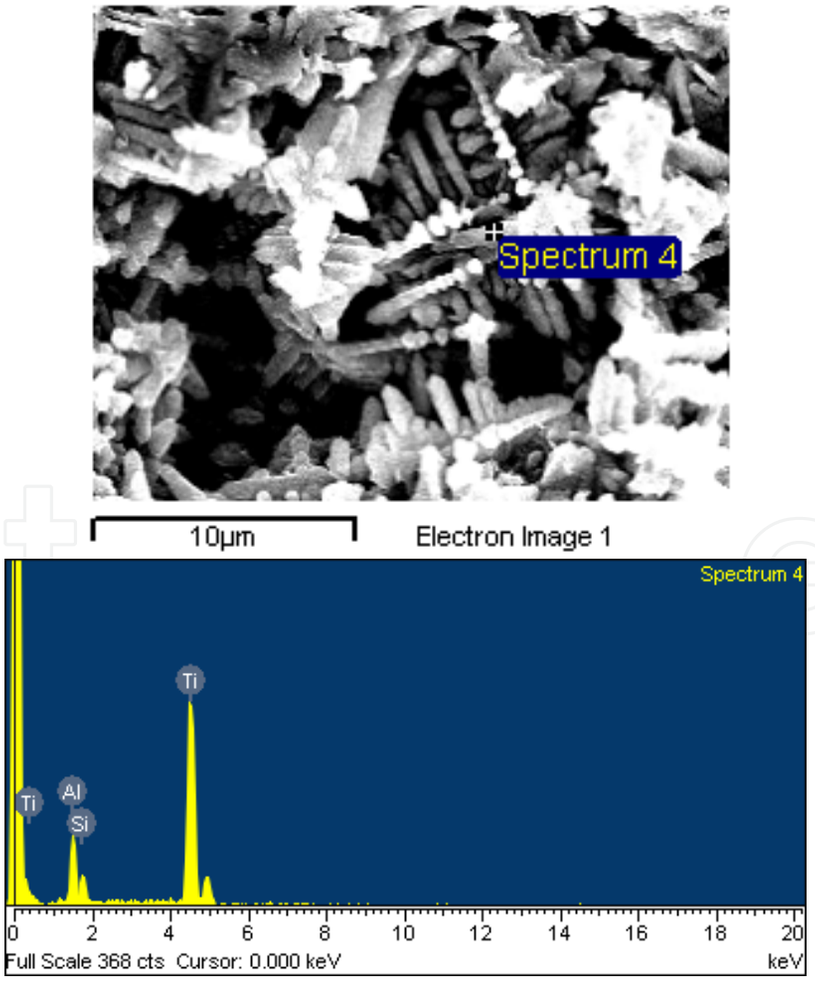

Figure 24. Microstructure and EDX of laser weld with thick Ti filler

Figure 24 shows the microstructure of laser welded joint with thick Ti filler and its corresponding energy dispersive X-ray spectroscopy (EDX) results. It can be observed that a large number of columnar Ti crystallization is distributed in the weld. From Figs. 23 and 24, it elucidates that with the increase of Ti thickness, the heat input into the substrate is decreased and most of energy is used for melting Ti led to the insufficient *in situ* reaction and stirring in the welding pool resulted in lower properties of welded joints.

Furthermore, in order to verify the temperature field, noncontact thermometer (model AZ9881) was used to measure the spot temperature on-line. The measured temperature results are shown in Fig. 25. It shows that the measured results agree well with the simulated results.

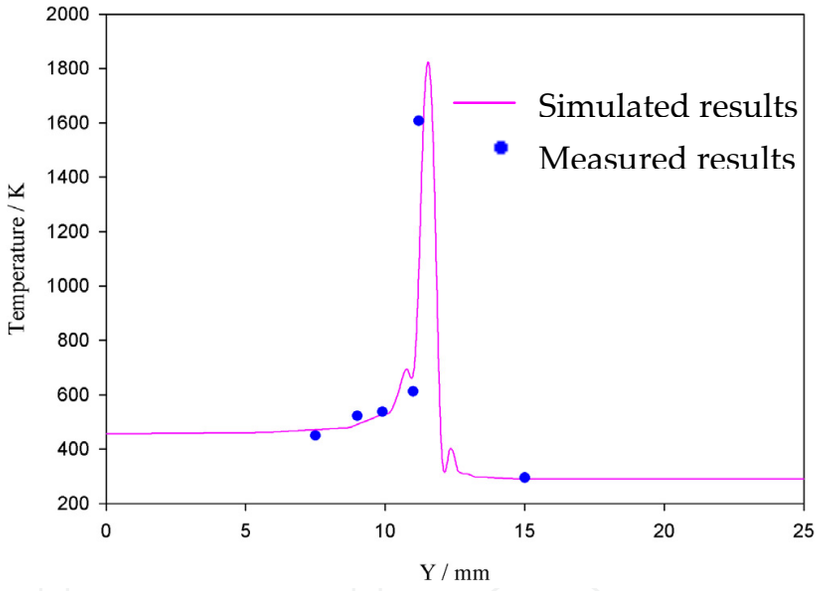

Figure 25. Surface temperature distribution in the processing center

4.3. Microstructure evolution simulation

According to the temperature calculation, the simulation of the evolution of the microstructure based on thermodynamic equilibria, diffusion [5, 6, 7] was shown in Fig. 26. It showed that during the welding pool solidification, the *in situ* reinforcement particles TiC would be formed around the initial reinforcement SiC particles. With the increase of cooling time, the initial reinforcement SiC particles would be replaced by the newly-formed *in situ* reinforcement particles TiC. It was well matched with the results shown in Figs. 7 and 9.

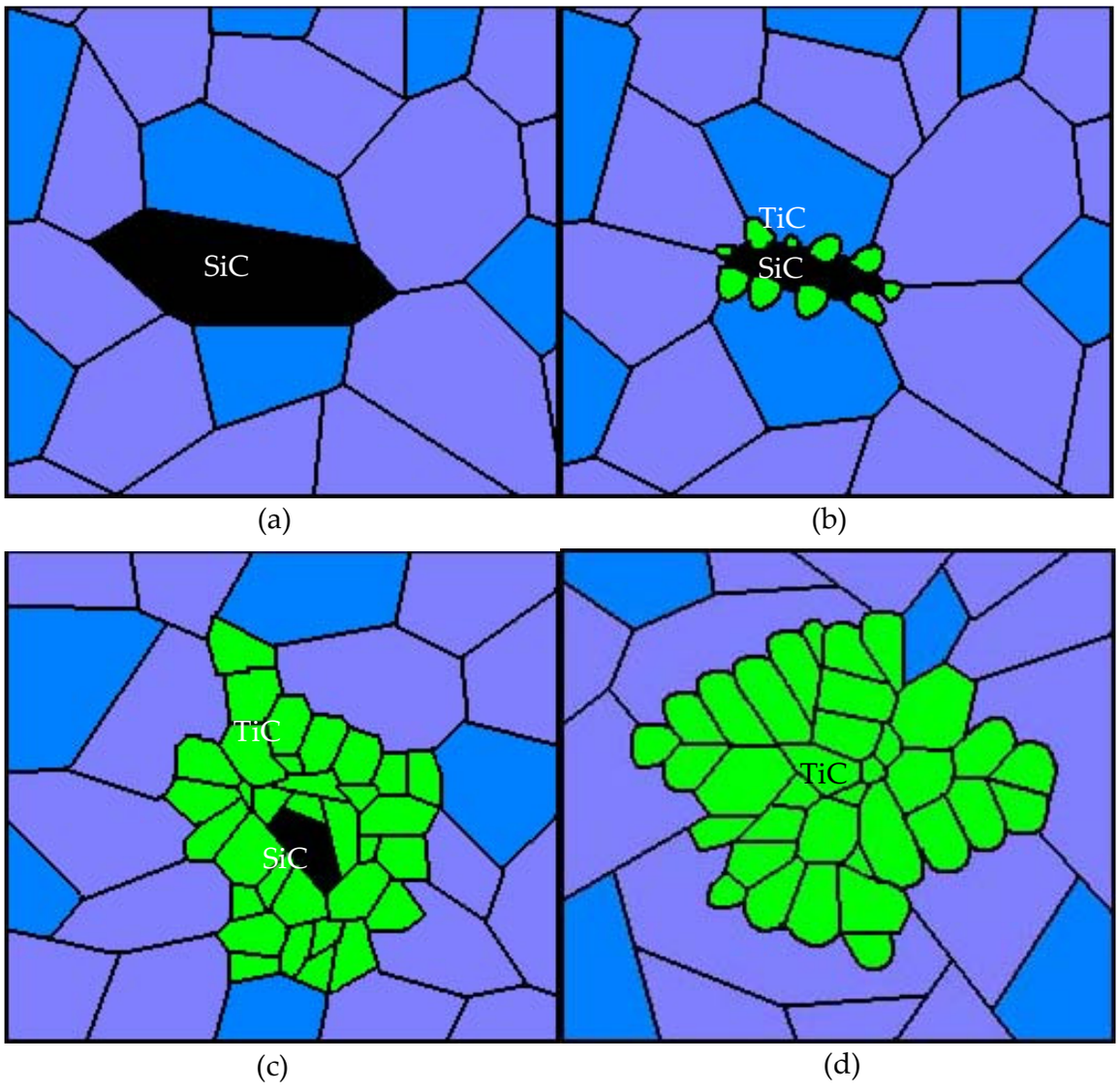

Figure 26. Simulation on microstructure evolution
(a) Initial (b) Start of solidification (c) Middle of solidification (d) End of solidification

5. Conclusions

The use of titanium as a filler metal in Nd:YAG laser welding of SiC_p/A356 provided beneficial *in situ* reinforcement effect. The effect of *in situ* reinforcement of the Ti filler allowed the newly-formed reinforcement TiC particles to distribute uniformly in the weld that subsequently resulted in successfully welding the SiC_p/A356 composite. Moreover, the typical pernicious interfacial reaction microstructure such as Al_4C_3 was effectively restrained from the interface between aluminum matrix and reinforcement particles in the Nd:YAG laser welding of SiC_p/A356 with Ti filler. Furthermore, according to the temperature calculation, the evolution of the microstructure was simulated based on thermodynamic equilibria, diffusion. Results were well matched with the corresponding experiments.

Author details

Kelvii Wei Guo
MBE, City University of Hong Kong, Hong Kong, China

Acknowledgement

The work is supported by a RGC general research fund (GRF) (Grant No.:9041503.) and a Strategic Research Grant (SRG) from City University of Hong Kong (Grant No.: 7002287.)

6. References

[1] J. M. Go´mez de Salazar, M. I. Barrena: Dissimilar Fusion Welding of AA7020/MMC Reinforced with Al_2O_3 Particles. Microstructure and mechanical properties. Materials Science and Engineering A 2003; 352(1-2): 162-168.
[2] W. Guo, M. Hua, H. W. Law and J. K. L. Ho: Liquid-Phase Impact Diffusion Welding of SiCp/6061Al and Its Mechanism. Materials Science and Engineering: A, 2008, 490, (1-2), 427-437.
[3] W. Guo, M. Hua, and J. K. L. Ho: Study on Liquid-Phase-Impact Diffusion Welding SiCp/ZL101. Compos. Sci. Technol., 2007, 67, (6), 1041-1046.
[4] L. M. Marzoli, A. V. Strombeck, J. F. Dos Santos, C. Gambaro, L. M. Volpone: Friction Stir Welding of an AA6061/Al2O3/20p Reinforced Alloy. Composites Science and Technology 2006; 66(2): 363-371.
[5] D. A. Porter, K. E. Easterling: Phase Transformations in Metals and Alloys, 2nd. Cheltenham: Nelson Thornes, 2001.
[6] R. Riedel: Handbook of Ceramic Hard Materials. New York: Wiley-VCH, Weinheim, 2000.
[7] R. Boyer, G. Welsch, E. W. Collings: Materials Properties Handbook: Titanium Alloys. Materials Park, Ohio: ASM International, 1994.
[8] J. R. Davis: ASM Specialty Handbook – Aluminum and Aluminum Alloys. Materials Park, Ohio: ASM International, 1993. p.557.
[9] S. Mall, T. Nicholas: Titanium Matrix Composites – Mechanical Behavior. Lancaster, Pa.: Technomic Pub. Co. Inc., 1998.
[10] W. M. Steen: Laser Material Processing, 3rd ed. London: Springer-Verlag; 2003.
[11] K. W. Guo: Influence of In Situ Reaction on the Microstructure of SiCp/AlSi7Mg Welded by Nd:YAG Laser with Ti Filler. J. Materials Engineering and Performance, 2010, 19, 52-58.
[12] A.F. Mills: Heat and Mass Transfer. P. R. Donnelly & Sons Company; 1995.